BIOCHEMISTRY
including biophysical chemistry & molecular biology
Article

Biochemistry **2009,** *48,* 10665–10678 10665
DOI: 10.1021/bi9010682

Importance of the Conserved Lysine 83 Residue of *Zea mays* Cytochrome b_{561} for Ascorbate-Specific Transmembrane Electron Transfer As Revealed by Site-Directed Mutagenesis Studies[†]

Nobuyuki Nakanishi,[‡] Motiur Md. Rahman,[‡] Yoichi Sakamoto,[§] Tadakazu Takigami,[∥] Kazuo Kobayashi,[⊥] Hiroshi Hori,[#] Toshiharu Hase,[△] Sam-Yong Park,[◇] and Motonari Tsubaki*[,§]

[‡]*Department of Molecular Science and Material Engineering, Graduate School of Science and Technology and* [§]*Department of Chemistry, Graduate School of Science, Kobe University, 1-1 Rokkodai-cho, Nada-ku, Kobe, Hyogo 657-8501, Japan,* [∥]*Department of Life Science, Graduate School of Science, Himeji Institute of Technology, Kamigoori-cho, Akou-gun, Hyogo 678-1297, Japan,* [⊥]*Institute of Scientific and Industrial Research, Osaka University, Mihogaoka 8-1, Ibaraki, Osaka 567-0047, Japan,* [#]*Division of Bioengineering, Department of Mechanical Science and Bioengineering, Graduate School of Engineering Science, Osaka University, Machikaneyama-cho, Toyonaka, Osaka 560-8531, Japan,* [△]*Institute for Protein Research, Osaka University, Suita, Osaka 565-0871, Japan, and* [◇]*Protein Design Laboratory, Division of Science of Biological Supramolecular Systems, Graduate School of Integrated Science, Yokohama City University, Yokohama, Kanagawa 230-0045, Japan*

Received June 26, 2009; Revised Manuscript Received October 4, 2009

ABSTRACT: Cytochromes b_{561}, a novel class of transmembrane electron transport proteins residing in a large variety of eukaryotic cells, have a number of common structural features including six hydrophobic transmembrane α-helices and two heme ligation sites. We found that recombinant *Zea mays* cytochrome b_{561} obtained by a heterologous expression system using yeast *Pichia pastoris* cells could utilize the ascorbate/mondehydroascorbate radical as a physiological electron donor/acceptor. We found further that a concerted proton/electron transfer mechanism might be operative in *Z. mays* cytochrome b_{561} as well upon the electron acceptance from ascorbate to the cytosolic heme center. The well-conserved Lys^{83} residue in a cytosolic loop was found to have a very important role(s) for the binding of ascorbate and the succeeding electron transfer via electrostatic interactions based on the analyses of three site-specific mutants, K83A, K83E, and K83D. Further, unusual behavior of the K83A mutant in pulse radiolysis experiments indicated that Lys^{83} might also be responsible for the intramolecular electron transfer to the intravesicular heme. On the other hand, pulse radiolysis experiments on two site-specific mutants, S118A and W122A, for the well-conserved residues in the putative monodehydroascorbate radical binding site showed that their electron transfer activities to the monodehydroascorbate radical were very similar to those of the wild-type protein, indicating that Ser^{118} and Trp^{122} do not have major roles for the redox events on the intravesicular side.

Cytochrome b_{561} exists in the neurosecretory vesicle membranes of the nervous system of higher animals. The cytochrome receives an electron equivalent from cytosolic ascorbate (AsA)[1] and donates it to the intravesicular monodehydroascorbate (MDA) radical to regenerate AsA after the transmembrane electron transfer (*1*−*4*). Two types of copper-containing monooxygenases, dopamine β-monooxygenase and peptidylglycine α-amidating monooxygenase, residing inside of the vesicles, then conduct hydroxylation reactions using two electron equivalents from AsA molecules and a dioxygen for the production of various neurotransmitters, such as noradrenaline and amidated neuropeptides (*5*−*8*). Therefore, the transmembrane electron transfer catalyzed by cytochrome b_{561} is essential for the biosynthesis of the neurotransmitters. To perform such a unique electron transfer, cytochrome b_{561} has very different characters from those of usual cytochromes. (a) It has a 6-transmembrane α-helix structure with a very hydrophobic nature (*9*, *10*) and is, therefore, very difficult to be purified into a homogeneous state. (b) It has two heme *b* centers in a molecule (*11*) with one residing on the cytosolic side and the other locating on the intravesicular side, respectively (*10*). Probably, this type of topology is necessary to conduct an efficient transmembrane electron transfer. (c) Two heme *b* centers have different redox potentials from each other (*12*, *13*), and this difference is presumably required to exhibit the specificities for AsA and the MDA radical, respectively, and, therefore, to inhibit the reverse electron transfer. (d) Although both heme *b* groups are expected to have a bisimidazole-His coordination structure, their EPR characteristics are very different from each other (*11*, *14*). (e) Additionally, cytochrome b_{561} has two well-conserved sequences on the cytosolic and intravesicular side, respectively, of the molecule (*10*), and therefore, they are postulated as the binding sites for AsA and the MDA radical, respectively.

In the past, cytochrome b_{561} was believed to exist only in neuronal or neuroendocrine cells of higher animals, such as human and bovine, and as low as insects (*8*) and planarian (*15*).

[†]This work was supported by Grants-in-Aid for Scientific Research on Priority Areas (System Cell Engineering by Multiscale Manipulation, 18048030 and 20034034 to M.T.) from the Japanese Ministry of Education, Science, Sports, and Culture.

*Corresponding author. Tel: +81-78-803-6582. Fax: +81-78-803-6582. E-mail: mtsubaki@kobe-u.ac.jp.

[1]Abbreviations: AsA, ascorbate; MDA, monodehydroascorbate; Zmb_{561}, *Zea mays* cytochrome b_{561}; DEPC, diethyl pyrocarbonate; EPR, electron paramagnetic resonance, MALDI-TOF, matrix-assisted laser desorption/ionization time of flight; SDS−PAGE, sodium dodecyl sulfate−polyacrylamide gel electrophoresis.

Published on Web 10/05/2009

Recently, a new member of this protein family was found in the duodenal cells of the small intestine and was shown to have a ferric reductase activity for the trans-plasma membrane uptake of iron (*16*, *17*). However, as the genome projects for various organisms progressed, we began to realize that there were many genes encoding proteins homologous to animal cytochrome b_{561} (*18*) in a very wide range of higher plants, such as *Arabidopsis thaliana* (*19*, *20*), *Phaseolus vulgaris* (*21*), and *Citrullus lanatus* L. (*22*). There have been many reports concerning the purification of heme *b*-containing proteins being characterized by an α-band peak around 561 nm in the visible absorption spectra and high reducibility with AsA from various plants tissues (for a review, see ref *23*). These heme *b*-containing proteins are likely residing in the plasma membranes (*24*−*28*) and are possibly a member of the cytochrome b_{561} protein family. However, information regarding these new members of cytochrome b_{561} in plant tissues is still very scarce. Practically, we do not know anything about their physiological roles, 3D structures, and distribution in the plant body or even within the cells, although several pieces of evidence indicated that at least some parts of plant cytochromes b_{561} might locate in tonoplast membranes (*29*−*31*) instead of plasma membranes (*22*).

In the present study, we conducted very comprehensive analyses on cytochrome b_{561} from maize (*Zea mays*) including its molecular cloning, functional heterologous expression in methylotrophic yeast *Pichia pastoris* cells (*32*), purification, biochemical and biophysical characterization, and site-directed mutagenesis analyses.

MATERIALS AND METHODS

Site-Directed Mutagenesis. The cloned full-length Zmb_{561} (AB182641; DDBJ/EMBL/GenBank) was ligated into the *Eco*RI-*Xba*I site of the pPICZB vector, as described in Supporting Information. Site-specific mutations were introduced by using the QuickChange II site-directed mutagenesis kit (Stratagene Corp., La Jolla, CA). All of the primers used for the mutagenesis are listed in Supporting Information Table S1. Four mutants (K83A, K83E, K83E, S118A) without a 6×His tag moiety and one mutant (W122A-H_6) with a C-terminal 6×His tag were constructed. These constructs were each confirmed by DNA sequencing (ABI 3100 genetic analyzer; Applied Biosystems, Foster City, CA).

Preparation of the P. pastoris Microsomal Fraction. The cultured cells were centrifuged at 8000 rpm (8370*g*) (Hitachi CR 20G centrifuge) for 10 min at room temperature. The pelleted cells were suspended in buffer A (50 mM potassium phosphate buffer, pH 6.0, 2.0 M sorbitol, 0.1 mM dithiothreitol, 0.1 mM EDTA). To the suspension, zymolyase (from *Arthrobacter luteus*) (Seikagaku Corp., Tokyo, Japan) was directly added to 0.5 mg/mL, and the mixture was incubated for 3 h at 30 °C with shaking at 240 rpm. The mixture was centrifuged at 5000 rpm (3000*g*) for 10 min at 4 °C. The pellets were resuspended in buffer B (50 mM potassium phosphate buffer, pH 7.0, 0.65 M sorbitol, 0.1 mM dithiothreitol, 0.1 mM EDTA, 1.0 mM PMSF). Then, the suspension was sonicated with an Astrason S3000 ultrasonic processor (Misonix Inc., Farmingdale, NY) at 48 W (with duty cycle of 50%) for 3.0 min on ice and was centrifuged at 10000 rpm (12000*g*) for 10 min at 4 °C. The supernatant was ultracentrifuged at 30000 rpm (104000*g*) (Hitachi CP 70MX ultracentrifuge) for 60 min at 4 °C. The resultant pellet was resuspended in 50 mM potassium phosphate buffer, pH 7.0, containing 10% (w/v) glycerol. This yeast microsomal fraction was saved at −80 °C until use.

Solubilization of Microsomal Membranes and Purification of the Z. mays Cytochrome b_{561} Protein. The intact (WT-Zmb_{561}) and 6×His-tagged Zmb_{561} (WT-Zmb_{561}-H_6) were purified as follows. Membrane fractions (∼3.5 mg of protein/mL) containing Zmb_{561} (WT-Zmb_{561} or WT-Zmb_{561}-H_6) were solubilized with 1.0% (w/v) *n*-octyl β-glucoside (Anatrace, Maumee, OH) in 50 mM potassium phosphate buffer (pH 7.0), 10% (v/v) glycerol, and 1.0 mM sodium ascorbate. After being stirred at 4 °C for 3 h, the solubilized extract was centrifuged at 20000 rpm (48000*g*) (Hitachi CR 20G centrifuge) for 20 min, and the supernatant was saved. The supernatant was concentrated to ∼2 mL with a 50 mL Amicon concentrator (using a membrane of MWCO = 30000) (Millipore, Billerica, MA).

For the purification of WT-Zmb_{561}, a following procedure was used. The concentrated protein solution was loaded onto a DEAE-Sepharose CL-6B (Amersham Biosciences, GE Healthcare Bio-Sciences) ion-exchange column equilibrated with 40 mM potassium phosphate buffer (pH 7.0) containing 1.0% (w/v) *n*-octyl β-glucoside and 1 mM sodium ascorbate. WT-Zmb_{561}-rich fractions were collected, concentrated, and directly applied onto a ConA−Sepharose (Amersham Bioscience) column equilibrated with 50 mM potassium phosphate buffer (pH 7.0) containing 1.0% (w/v) *n*-octyl β-glucoside to remove contaminants, and the pass-through fraction was saved.

For the purification of WT-Zmb_{561}-H_6, a following procedure was used. The concentrated protein solution was loaded onto a DEAE-Sepharose CL-6B column preequilibrated with 35 mM potassium phosphate (pH 7.0) buffer. The column was washed with 35 mM potassium phosphate (pH 7.0) buffer containing 1% *n*-octyl β-glucoside and 1 mM AsA. The absorbed WT-Zmb_{561}-H_6 was slowly eluted during the washing, and the WT-Zmb_{561}-H_6-rich fractions were collected and concentrated. During this ion-exchange chromatography step, Western blotting analyses were made occasionally using rabbit IgG antibodies (Takara-Bio, Ohtsu, Japan) raised against the C-terminal part of WT-Zmb_{561} to ensure that all of the expressed Zmb_{561} protein was recovered. The concentrated sample was supplemented with 300 mM NaCl and 10 mM imidazole, and the mixture was applied to a 5 mL Ni^{2+}-NTA agarose (QIAGEN, Hilden, Germany) column which had been preequilibrated with buffer A (50 mM potassium phosphate buffer, pH 7.0, containing 1% *n*-octyl β-glucoside, 10% glycerol, 300 mM NaCl, and 1.0 mM AsA) containing 10 mM imidazole. The column was washed with a 20 bed volume of buffer A containing 20 mM imidazole, and then WT-Zmb_{561}-H_6 protein was eluted with buffer A containing 250 mM imidazole. Imidazole in the sample solution was removed by gel filtration using a PD-10 mini column preequilibrated with 50 mM potassium phosphate buffer (pH 7.0) containing 1.0% (w/v) *n*-octyl β-glucoside.

Concentrations of the purified WT-Zmb_{561} and WT-Zmb_{561}-H_6 were determined spectrophotometrically using a difference extinction coefficient of 27.7 mM^{-1} cm^{-1} at 561 nm *minus* 575 nm in the reduced state (*11*). Final protein concentration was determined by the modified Lowry method (*33*) using bovine serum albumin as a standard.

N-Terminal Amino Acid Sequencing of the Purified Cytochrome b_{561}. Purified Zmb_{561} (16 μg) was separated on SDS−PAGE followed by an electroblotting onto a PVDF membrane (Immobilon PSQ; Millipore, Billerica, MA). The transferred protein band visualized by Ponceau-S staining was

excised from the membrane and was analyzed with an ABI protein sequencer (Procise 492; Applied Biosystem, Foster City, CA) up to 10 cycles.

Production of Anti-C-Terminal Peptide Antibody. The C-terminal peptide (^{214}DLVAAIAPVRLEEPQGYDPIPEN^{236}) of Zm*b*561, that is considered to be exposed on the cytosolic side of the membranes, was overexpressed in *Escherichia coli* (XL1-Blue) as a fusion protein with the 6×His-tagged dihydrofolate reductase (DHFR) protein by employing a QIAexpress expression system (pQE-41; QIAexpress type II kit; QIAGEN, Hilden, Germany) (Supporting Information Figure S4). The first and second Val residues in the C-terminal peptide, corresponding to positions 214 and 215 of Zmb_{561}, were artificially changed to Asp-Leu, as indicated above, to make an appropriate fusion with the DHFR moiety at its C-terminus. The fusion protein was highly purified according to the recommended protocol. The purified protein was emulsified in Freund's complete (initial) or incomplete (booster) adjuvant and was injected subcutaneously into a female Japanese White rabbit. After several booster injections, blood was collected (Takara-Bio, Ohtsu, Japan). Polyclonal antibodies against the C-terminal peptide of Zmb_{561} were then purified according to the published procedure.

Western Blot Analysis. Purified protein samples were separated by 15% SDS−PAGE according to the Laemmli method (*34*). The protein in the gel were transferred onto a PVDF membrane with a Trans-blot Transfer medium (Bio-Rad Laboratories, Inc., Hercules, CA) by using Power Pac (Bio-Rad Laboratories, Inc., Hercules, CA) in 20 mM glycine, 25 mM Tris, and 20% methanol. The rabbit IgG fraction raised against the native form of the C-terminal part of Zmb_{561} as described above was used as a primary antibody. The Zmb_{561} protein−primary antibody complex was detected by anti-rabbit IgG horseradish peroxidase-conjugated secondary antibodies obtained from goat (Wako Pure Chemical Industries, Ltd., Osaka, Japan) using 4-chloro-1-naphthol and hydrogen peroxide as substrate.

MALDI-TOF Mass Spectrometry. Mass spectrometric analyses were carried out on a Voyager DE Pro mass spectrometer (Applied Biosystem, Foster City, CA) using a 20 kV accelerating voltage. The mass spectra were acquired by adding the individual spectrum from 256 laser shots. For protein analysis the samples were run in a linear mode and for peptide analysis in a reflector mode. The protein solutions were diluted 1:9 (v/v) with a matrix solution, 3,5-dimethoxy-4-hydroxycinnamic acid (Aldrich, Gillingham, England), 50 mg/mL in 30% acetonitrile in 0.3% TFA. The Zmb_{561} protein (50−100 μM; WT-Zmb_{561} or WT-Zmb_{561}-H_6 and its site-directed mutants (K83A, K83E, K83D, S118A, W122A-H_6)) was digested either with TPCK-treated trypsin (0.01 mg/mL) or *Staphylococcus aureus* V8 protease (0.01 mg/mL), respectively. After 48 h of incubation at room temperature, the peptide solutions were diluted 1:9 (v/v) with a matrix solution, α-cyano-4-hydroxycinamic acid (Aldrich, Gillingham, England), 50 mg/mL, in 50% acetonitrile in 0.3% TFA. The mixtures (typically, 1.0 μL) were deposited on the sample plate and allowed to air-dry before analysis. The search of the corresponding fragments in the amino acid sequence of Zmb_{561} was carried out using the program GPMAW (version 6.11) (Lighthouse Data, Odense M, Denmark). Molecular masses of the observed polypeptides matched the theoretical ones within accuracy of 0.1% or better.

Measurement of EPR Spectra. Purified Zmb_{561} samples (WT-Zmb_{561}, ~400 μM) in 50 mM potassium phosphate (pH 7.0) buffer containing 1.0% (w/v) *n*-octyl β-glucoside were introduced into EPR tubes and were frozen in liquid nitrogen (77 K) immediately. EPR measurements were carried out at X-band (9.23 GHz) microwave frequency using a Varian E-12 EPR spectrometer with 100 kHz field modulation, as previously described (*11*). An Oxford flow cryostat (ESR-900) was used for the measurements at 5 and 15 K. The microwave frequency was calibrated with a microwave frequency counter (Takeda Riken Co., Ltd., model TR5212). The magnetic field strength was determined by nuclear magnetic resonance of protons in water. Accuracy of the *g*-values was approximately ± 0.01

Pulse Radiolysis. Pulse radiolysis experiments were performed with an electron linear accelerator facility at the Institute of Scientific and Industrial Research, Osaka University, as previously described (*4*). The pulse width and energy were 8 ns and 27 MeV, respectively. The sample was placed in the quartz cell with an optical path length of 1.0 cm. The temperature of the sample was maintained at 20 °C. The light source for a spectrophotometer was a 150 W halogen lamp. After passing through the optical path, the transmitted light intensities were analyzed and monitored by a fast spectrophotometric system composed of a Nikon monochromator, an R-928 photomultiplier, and a UNISOKU data analyzing system (UNISOKU Co. Ltd., Osaka, Japan). The concentration of the MDA radical generated by pulse radiolysis was estimated from the absorbance at 360 nm, using a molar extinction coefficient of 3.3 mM^{-1} cm^{-1}. This concentration could be adjusted by varying the dose of electron beams. The 10 mM potassium phosphate buffer (pH 7.0) containing 1.0% *n*-octyl β-glucoside and 10 mM AsA was bubbled with N_2O gas for 5 min. Protein solutions were then prepared by diluting the concentrated Zmb_{561} solution to 4−6 μM with the buffer pretreated with N_2O gas.

Stopped-Flow Analysis. Rapid kinetic measurements were carried out using an RSP-100-03DR stopped-flow rapid-scan spectrometer (UNISOKU Co. Ltd., Osaka, Japan), as previously described (*35*). One chamber of the apparatus contained the oxidized form of WT-Zmb_{561} or WT-Zmb_{561}-H_6 (2.0 μM or as indicated in the text) in 50 mM sodium acetate (pH 5.0) or 50 mM potassium phosphate (pH 6.0, 7.0) buffer containing 1.0% *n*-octyl β-glucoside. The other chamber contained a test concentration of sodium ascorbate (AsA) (2, 4, 8, 16 mM) in the same buffer. The temperature of both chambers and the sample holder was maintained at 20 °C by connecting to a thermobath (Model NCB-1200; Tokyo Rikakikai Co., Ltd., Tokyo, Japan). The mixing was carried out with a 1:1 (v/v) ratio. Heme reduction of Zmb_{561} was followed spectrophotometrically by the absorbance change at 427 nm using a photomultiplier (single-wavelength mode). Data points were collected every 2.5 ms during the 10 s measurements for the singe-wavelength mode (total 4000 data points). The time courses of the absorbance change at 427 nm were fitted by use of a nonlinear least-squares method of a built-in software of the apparatus with a single (or a linear combination of) exponential decay equation.

Redox Titrations. Spectroscopic titrations were performed essentially as described by Dutton (*36*) and Takeuchi (*13*) using a Shimadzu UV-2400PC spectrometer equipped with a thermostated cell holder connected to a low-temperature thermobath (NCB-1200; Tokyo Rikakikai Co., Ltd., Tokyo, Japan). A custom anaerobic cuvette (1 cm light path, 5 mL sample volume) equipped with a combined platinum and Ag/AgCl electrode (6860-10C; Horiba, Tokyo, Japan) and a screw-capped side arm was used. The purified Zmb_{561} sample or its site-specific mutants (final, 5−10 μM) in 50 mM potassium phosphate buffer

(pH 7.0) containing 1.0% (w/v) *n*-octyl β-glucoside was mixed with redox mediators (potassium ferricyanide, 60 μM; quinhydrone, 20 μM; 1,2-naphthoquinone, 20 μM; phenazine methosulfate, 20 μM; duroquinone, 40 μM; 2-hydroxy-1,4-naphthoquinone, 5 μM; riboflavin, 20 μM). The sample was kept under a flow of moistened argon gas to exclude dioxygen and was continuously stirred with a small magnetic stirrer (CC-301; SCINICS, Tokyo, Japan) inside. Reductive titration was performed at 25 °C by addition of small aliquots of sodium dithionite (5 or 20 mM) solution through a needle in the rubber septum on the side arm; for a subsequent oxidative titration, potassium ferricyanide (5 or 20 mM) was used as the titrant. In an appropriate interval, visible absorption spectra and redox potentials were recorded. The changes in absorbance ($A_{561.0}$ minus $A_{567.2}$, the isosbestic point of Zmb_{561}) were corrected with the dilution effect and analyzed with Igor Pro (v. 6.03A2) employing a Nernst equation with a single or two redox components.

RESULTS

Analysis of the Deduced Amino Acid Sequence of Z. mays Cytochrome b_{561}. The deduced amino acid sequence of the full-length cDNA of Zmb_{561} encodes a 236 amino acid open reading frame with a theoretical molecular weight of 25424.52 (Supporting Information Figure S5). The length of the open reading frame (Supporting Information Figure S3) and the molecular weight were usual as a member of the cytochrome b_{561} family (Supporting Information Figure S5) (*37*). Hydropathy plot analysis was conducted based on the Kyte and Doolittle method (*38*) with an averaging window size of either 6 or 20 amino acid residues. Both results showed the presence of six membrane-spanning α-helices (Supporting Information Figure S6). ClustalW (v.1.80) analysis was performed on the DDBJ server, and Phylip format tree outputs from the ClustalW analysis were visualized using TreeViewPPC (v.1.6.6) based on the distance matrix using the neighbor-joining method. Phylogenetic analysis on the amino acid sequences of cytochromes b_{561} from various animals and plants (*39*) (Supporting Information Figure S7) showed that Zmb_{561} could be classified as a member of a subfamily comprising plant cytochromes b_{561}, which was clearly distinct from the animal cytochrome b_{561} protein subfamily residing in the neuroendocrine vesicles (*10*, *15*). Indeed, the amino acid sequence of Zmb_{561} showed only 32% identity to bovine adrenal cytochrome b_{561}. Zmb_{561} was also very distant from a subfamily of Dcytbs (*16*, *40*) and from a newly found subfamily consisting of b_{561}human3 and TSFhuman (*37*) with an unknown physiological function(s). Further, there were five fully conserved His residues (His^{52}, His^{86}, His^{108}, His^{120}, and His^{159}) as observed for animal cytochromes b_{561} (*10*); among them, two pairs (His^{52} and His^{120}; His^{86} and His^{159}) are assigned for axial ligands of the two heme centers (Supporting Information Figures S5 and S8) (*10*), and this assignment was confirmed recently by site-directed mutagenesis studies (*41*, *42*). In addition, the potential MDA radical binding motif -xYSLHSWxGx- with x being a hydrophobic amino acid in most of the family members (*10*) was clearly conserved in the Zmb_{561} sequence (^{116}LYSLHSWIGI^{125}) (Supporting Information Figure S5). The degree of the conservation for the other predicted AsA-binding sequence (ALLVYRVFR in the mammalian chromaffin cytochrome b_{561}) was somewhat lower (^{67}AIMVYRVLP^{75}). In addition to these conserved structural features, all cytochromes b_{561} aligned in Supporting Information Figure S5 showed strict conservation of five Gly, two Pro, one Gln, and one Lys residues. Further, there were several well-conserved aromatic residues, such as Trp^{30}, Phe^{49}, Tyr^{131}, and Trp^{135} (Supporting Information Figure S5). These aromatic residues were proposed previously to have a role(s) for mediating the electron transfer between the two heme prosthetic groups or a structural role to maintain the proper bundling of α-helices in the membranes (*10*).

Heterologous Expression and Purification of Z. mays Cytochrome b_{561}. Two forms of the recombinant Zmb_{561} (WT-Zmb_{561} and WT-Zmb_{561}-H_6) were each expressed successfully in yeast *P. pastoris* cells under the control of a methanol-inducible promoter (*AOX1*) (*32*) with a low-temperature incubation (30 °C). The expression level of Zmb_{561} varied between cultures, but based on the visible absorption redox difference spectra of the microsomal fraction, about 70 nmol of Zmb_{561}/100 mL of culture medium was attained. This expression level was sufficient for the extensive purification and for the biochemical and biophysical analyses on the purified proteins.

For the solubilization of Zmb_{561} in the microsomal membrane fraction, we used *n*-octyl β-glucoside at the concentration of 1.0% (w/v). At this concentration, almost all Zmb_{561} protein was extracted from the membranes, as observed for the purification of bovine adrenal cytochrome b_{561} (*11*). The solubilized Zmb_{561} was purified using DEAE-Sepharose ion-exchange column chromatography followed by affinity column chromatography (ConA−Sepharose column chromatography for WT-Zmb_{561} and Ni^{2+}-NTA agarose column for WT-Zmb_{561}-H_6) (Figure 1A). In the final stage of the purification, we could obtain about 40 nmol of purified Zmb_{561} protein starting from 100 mL scale cultivation.

Structural Analysis of the Recombinant Z. mays Cytochromes b_{561}. Both SDS−PAGE and Western blot analyses of the purified WT-Zmb_{561} (and WT-Zmb_{561}-H_6, not shown) showed smeared protein bands around 25 kDa (Figure 1A). Although the deduced amino acid sequence of Zmb_{561} contained two potential N-glycosylation sites (^{109}NES^{111} and ^{203}NFT^{205}) (Supporting Information Figure S5), periodic acid−Schiff (PAS) staining (*43*) of the purified WT-Zmb_{561} in SDS−PAGE gels did not show any indication of glycosyl groups. N-Terminal protein sequencing analyses for both of the purified samples (WT-Zmb_{561} and WT-Zmb_{561}-H_6) showed an identical sequence of GLGLGVRAAP, which corresponded to 2−11 residues of the deduced amino acid sequence of wild-type Zmb_{561}. This result indicated that only the N-terminal Met residue was removed posttranslationally. The possibility of the partial proteolytic digestion at the C-terminal part of WT-Zmb_{561} after the heterologous translation event was ruled out, since the entire protein band had a similar staining reactivity upon the Western blotting analysis (results not shown) using rabbit anti-C-terminal-peptide IgG antibodies (Supporting Information Figure S4). Other possible posttranslational modification(s) were also ruled out based on MALDI-TOF mass spectrometric analyses (Supporting Information Figures S9 and S10 and Tables S2 and S3). Therefore, we considered that the smearing of the protein bands of WT-Zmb_{561} and WT-Zmb_{561}-H_6 in SDS−PAGE gel (Figure 1A) might be due to the intrinsic property of this particular class of plant membrane proteins.

MALDI-TOF mass spectra of intact Zmb_{561} (WT-Zmb_{561} and WT-Zmb_{561}-H_6) in the presence of 1% *n*-octyl β-glucoside were analyzed in a linear mode (spectra not shown). The mass spectra for WT-Zmb_{561}-H_6 showed a clear molecular ion [$M + H^+$] peak at 26176.85 (m/z) slightly lower than the theoretical value of

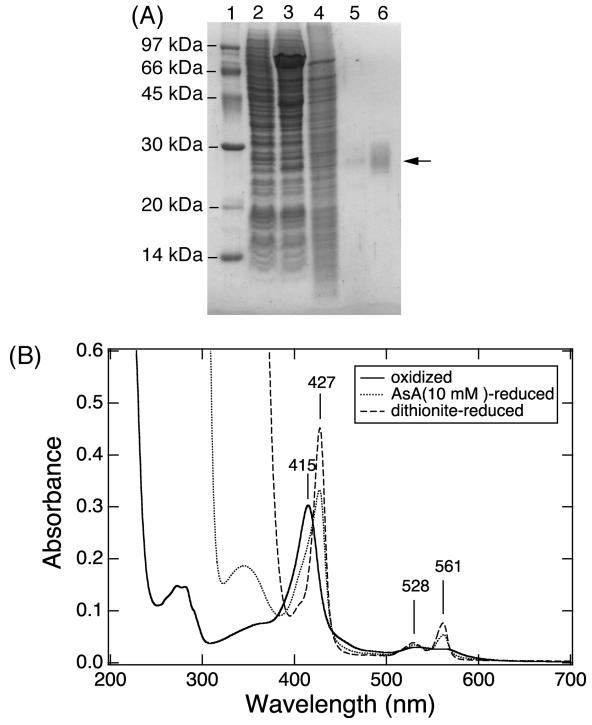

FIGURE 1: SDS−PAGE analysis (A) and UV−visible absorption spectra (B) of the purified recombinant WT-Zmb_{561}. (A) Heterologously expressed WT-Zmb_{561} samples in different purification stages were analyzed by 15% SDS−PAGE. Lane 1, molecular weight marker; lanes 2 and 3, 0 and 96h after the induction with MeOH; lane 4, microsomal fraction; lane 5, eluted fraction from DEAE-Sepharose column; lane 6, pass-through fraction from ConA−Sepharose column. An arrow indicates purified WT-Zmb_{561}. (B) Visible absorption spectra of the purified WT-Zmb_{561} in 50 mM potassium phosphate buffer, pH 7.0, containing 1.0% (w/v) *n*-octyl β-glucoside. The absorption spectra of oxidized, AsA (10 mM) reduced, and dithionite-reduced forms were recorded in a region from 700 to 300 nm (or to 200 nm for oxidized form) at room temperature.

26247.84, supporting the notion that the first Met residue was removed posttranslationally. The molecular ion [M + H^+] peak for WT-Zmb_{561} could not be identified, probably due to its stronger hydrophobic nature. MALDI-TOF mass spectrometric analyses on the tryptic and V8 protease peptides of WT-Zmb_{561} and WT-Zmb_{561}-H_6 proteins showed many partially cleaved polypeptides (Supporting Information Figures S9 and S10). We could identify most of these polypeptides. The identified peptides covered 2−236 residues for both tryptic and V8 protease peptides of WT-Zmb_{561}, whereas for WT-Zmb_{561}-H_6, tryptic peptides and V8 protease peptides covered 2−235 and 2−242 residues, respectively (Supporting Information Tables S2 and S3). It must be mentioned that we could not identify peptides containing the initiation Met residue, consistent with the results of N-terminal protein sequencing analyses. In addition, we found that there was neither undesirable mutation nor any other type(s) of posttranslational modification.

Spectroscopic and Electrochemical Properties of Purified Z. mays Cytochromes b_{561}. Purified Zmb_{561} (both WT-Zmb_{561} and WT-Zmb_{561}-H_6) showed characteristic visible absorption spectra with peaks at 415 nm for the oxidized form and at 561, 528, and 427 nm for the dithionite-reduced form (Figure 1B), very similar to those of bovine adrenal cytochrome b_{561} (*11*). The shape of the α-band peaked at 561 nm showed an asymmetric character, as found for bovine adrenal cytochrome b_{561} (*11*). Additions of AsA (10 mM) to oxidized WT-Zmb_{561} and WT-Zmb_{561}-H_6 caused a quick reduction of heme *b* reaching the final reduction level of ∼80%, suggesting that Zmb_{561} might utilize AsA as a physiological reductant in maize cells.

A part of the potentiometric behavior of visible absorption spectra of Zmb_{561} is shown in Figure 2A. The intensity of the α-band peak at 561 nm increased as the redox potential decreased with a clear isosbestic point around 567.2 nm. In a lower wavelength region (around the β-band region), such isosbestic points were not so clear due to the progression in absorbance of mediators included in the medium. The apparent midpoint potential was estimated as +66 mV (Figure 2B, C), about 60 mV lower than the corresponding values of bovine adrenal cytochrome b_{561} (+125 mV) for the purified sample of our own (*13*) and others (*44*) and for the membrane preparations (*45*, *46*). The Nernst plot (i.e., redox potential vs log([ox]/[red]) of the data showed a slope with 83 mV at the center region, which is much greater than the 59 mV predicted by the Nernst equation with a single redox component (Figure 2C). However, the lower asymptotic potentials in the plot could not be directly estimated due to poor quality of the data. All of the data points were then curve-fitted with a least-squares method assuming two distinct redox components (Figure 2B). Results showed that the midpoint potential of the higher and the lower redox components had +119 and +11 mV, respectively (Table 1). The separation between the two estimated values was similar to a corresponding value previously estimated for bovine adrenal cytochrome b_{561} (+170 and +60 mV) (*13*). We did not observe any meaningful differences between WT-Zmb_{561} and WT-Zmb_{561}-H_6; the former showed its apparent midpoint potential as +64 mV and its higher and lower redox components as +118 and +9 mV, respectively.

EPR spectra of oxidized WT-Zmb_{561} measured at 15 and 5 K showed two g_z signals (g_z = 3.69, 3.21) and one g_y signal (g_y = 2.27) (Supporting Information Figure S11A). Based on the comparison with the EPR spectra of bovine adrenal cytochrome b_{561} (*11*), the g_z = 3.69 species was assigned to the heme center on the cytosolic side and the species with g_z = 3.21 and g_y = 2.27 to the heme center locating on the other side, respectively. This result was consistent with our proposal of two independent heme species in a Zmb_{561} molecule on the basis of amino acid sequence analysis (*10*).

Stopped-Flow Analysis of Z. mays Cytochrome b_{561} for the Electron Acceptance from AsA. The electron-accepting ability of Zmb_{561} (WT-Zmb_{561} or WT-Zm b_{561}-H_6) from AsA was analyzed by stopped-flow spectrometry. Parts of the results are shown in Supporting Information Figure S12, in which absorbance changes at 427 nm after the mixing of oxidized WT-Zmb_{561}-H_6 (final 1 μM) with 8 mM AsA (final 4 mM) at three different pH (5.0, 6.0, 7.0) were presented. In the inset, the absorbance changes in a logarithmic time scale were shown (Supporting Information Figure S12, inset). At pH 7.0 and 6.0, there was a slight difference in the time courses of the reduction process of each other; at pH 6.0, it showed a slightly higher reduction rate. These reduction processes were not so much different from those of bovine adrenal cytochrome b_{561} measured at pH 7.0 and 6.0 (*47*). At pH 5.0, however, we observed significant retardation of the electron transfer from AsA to the oxidized heme center (Supporting Information Figure S12, inset). This unusual phenomenon was previously observed for bovine adrenal cytochrome b_{561} at pH 5.0 (and, with a lesser extent, at pH 5.5) (*47*). The extent of the retardation (or the time lag) was even stronger in the present case. On the other hand, the final

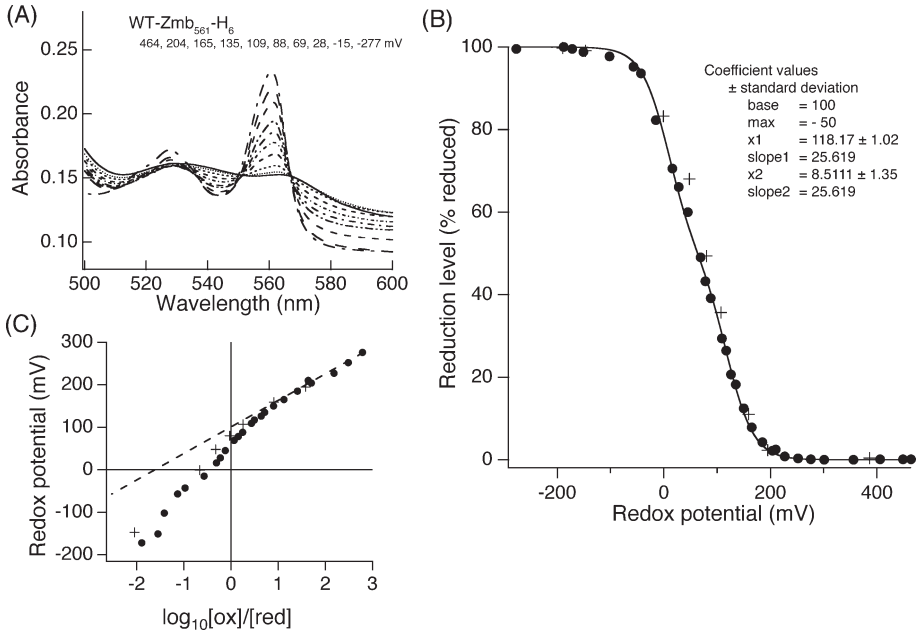

FIGURE 2: Potentiometric spectroscopic behavior of purified recombinant Zmb_{561} (A), a least-squares curve fitting of the data points (B), and a part of the Nernst plot of the redox titration data (C). (A) Absorption spectra of Zmb_{561} poised in various redox potentials were measured and plotted. Potentials are expressed relative to the normal hydrogen electrode (NHE). (B) Percentages of the heme reduction level were calculated based on the absorbance difference of the α-band peak (561.0 nm) and an isosbetic point (567.2 nm). Solid circles (●) and crosses (+) indicate data points for the reductive and the oxidative titrations, respectively. A least-squares curve fitting on the data points of the reductive phase was conducted by assuming two distinct redox components {i.e., with a linear combination of two sigmoid functions; $f(x)$ = base + (max*1/(1 + exp((x1 − x)/slope1))) + (max*1/(1 + exp((x2 − x)/slope2))), in which base, max, slope1, and slope2 were fixed as 100, −50, 25.62, and 25.62, respectively, during the curve-fitting procedure, and x1 and x2 gave the estimated midpoint potentials (in mV), respectively}. (Panel C) Nernst plot analysis for the reductive (solid circles ●) and oxidative (crosses +) titration of Zmb_{561} in comparison with the upper asymptotic potential line with a slope of 59 mV. Other details are described in the text.

Table 1: Redox Potentials of Zmb_{561} and Effects of Site-Specific Mutations on the Redox Properties in Comparison with Those of Bovine Adrenal Cytochrome b_{561}

cytochrome	app midpoint potential (mV)	slope[a]	estd higher midpoint potential[b] (mV)	estd lower midpoint potential[b] (mV)
WT-Zmb_{561}	+65.6	46.4	+118.9	+11.3
WT-Zmb_{561}-H_6	+64.0	46.3	+118.2	+8.5
K83A	+44.8	41.5	+93.0	−4.4
K83D	−40.3	66.7	+47.4	−130.0
K83E	+36.6	46.7	+90.4	−20.9
S118A	+43.2	47.7	+101.6	−14.5
W122A-H_6	+44.9	48.8	+104.1	−13.2
bovine b_{561}[c]	+125		+170	+60
bovine b_{561}[d]	+128		+170	+70

[a]Slope values were defined as variables during the fitting procedure using a single sigmoidal function and are, therefore, corresponding to the slope of the curvature. [b]For the curve-fitting procedure using two independent sigmoidal functions, the slope value for each sigmoidal function was fixed as 25.619 and is, therefore, not indicated. [c]From ref *44* for the purified form obtained from bovine adrenal gland. [d]From ref *13* for the purified form obtained from bovine adrenal gland.

reduction level was at most 65% at pH 5.0, slightly lower than that of bovine adrenal cytochrome b_{561}. It must be mentioned that the lower reducibility of the heme centers of Zmb_{561} at pH 5.0 was not due to the partial denaturation, since the dithionite reduction at pH 5.0 caused a 100% reduction of the heme showing an almost identical visible absorption spectrum with that measured at a neutral pH (Figure 3B).

Pulse Radiolysis Analysis. Pulse radiolysis experiments for the purified WT-Zmb_{561} were performed in the presence of AsA (10 mM). Within 10 ms after the generation of a pulse beam, we observed a very rapid decrease in absorbance at 425 nm and a concerted rapid increase in absorbance at 405 nm (Figure 4A,B). These absorbance changes were considered as rapid oxidation of the reduced heme center caused by the electron transfer to the MDA radical, which was produced by the pulse beam. Immediately after the oxidation of the heme center and within a following 2 s interval, the decreased absorbance at 425 nm recovered to the original level (Figure 4C), suggesting the rereduction of the oxidized heme centers by surrounding AsA. An apparent first-order rate constant for the initial electron donation to the MDA radical was 0.27×10^3 s^{-1} at pH 7.0 based on the decrease of A_{425} (Table 2), which was comparative with that of bovine adrenal cytochrome b_{561} under a similar experimental condition (*4*). As pH decreased, the apparent rate constant increased to 0.47×10^3 s^{-1} at pH 6.0 and to 0.66×10^3 s^{-1} at pH 5.0. When the analyses were made based on the increase of A_{405} (heme oxidation), almost identical results were obtained. This pH dependency was also very similar to that observed for bovine adrenal cytochrome b_{561} (*4*). This tendency is probably reflecting the optimal pH condition of Zmb_{561} for the efficient electron transfer to the MDA radical on the acidic intravesicular side. The oxidation of the intravesicular heme was a consequence of a bimolecular reaction of the MDA radical with Zmb_{561}, and therefore, the second-order rate constants could be calculated in relative ratios of the apparent rate constant to that of WT-Zmb_{561} measured under the similar experimental condition and was estimated as 1.0×10^7 M^{-1} s^{-1} (at pH 7.0).

The apparent rate constants for the following rereduction process were found to be 2.4 s^{-1} (pH 7.0), 5.5 s^{-1} (pH 6.0), and 4.6 s^{-1} (pH 5.0) based on the measurements at 425 nm (Table 2).

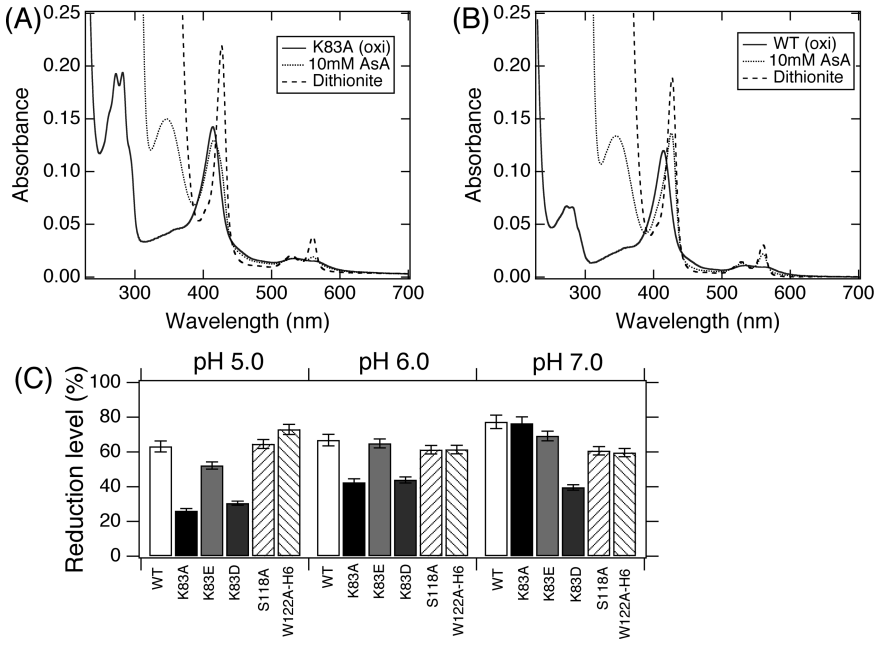

FIGURE 3: Absorption spectra of oxidized, AsA-reduced, and dithionite-reduced forms of K83A (A) and of WT-Zmb_{561} at pH 5.0 (B) and the final heme reduction levels of WT-Zmb_{561} and its mutants using AsA as a reductant (C). (A) After 30 min of incubation of K83A with AsA (10 mM) in 50 mM sodium acetate (pH 5.0) buffer containing 1.0% (w/v) *n*-octyl β-glucoside, its UV−visible absorption spectrum was recorded and was compared with those of K83A in oxidized and in dithionite-reduced forms. (B) After 30 min of incubation of WT-Zmb_{561} with AsA (10 mM) in 50 mM sodium acetate (pH 5.0) buffer containing 1.0% (w/v) *n*-octyl β-glucoside, its UV−visible absorption spectrum was recorded and was compared with those of WT-Zmb_{561} in oxidized and in dithionite-reduced forms. (C) The final heme reduction levels with AsA as a reductant were calculated at three different pH (5.0, 6.0, and 7.0) from the visible absorption spectra for WT-Zmb_{561} and its mutants (K83A, K83E, K83D, S118A, and W122A-H_6) based on their respective dithionite-reduced form as 100% reduced.

These values were also very similar to those of bovine adrenal cytochrome b_{561} (*4*) under similar experimental conditions. Taken together, the present results demonstrated that the electron transfer from the reduced heme center of Zmb_{561} to the MDA radical did take place on the intravesicular side and was followed by a transmembrane electron transfer from AsA on the cytosolic side. It must be noted, however, that there might be two processes being overlapped in the rereduction process, i.e., rereduction of oxidized heme with AsA and intramolecular heme-to-heme electron transfer (*4*).

Though the tissue or subcellular localization of Zmb_{561} in maize cells was not investigated in the present study, we tentatively call the electron acceptance site (from cytosolic AsA) "the cytosolic heme center" and the electron donation site (to the MDA radical) "the intravesicular heme center", hereafter, following the notation of bovine adrenal cytochrome b_{561} (*10*).

Rationale of the Mutational Analyses. In the next stage of our study, we focused on three amino acid residues with a high degree of conservation among the plant and animal cytochromes b_{561} (Supporting Information Figure S5) as targets for site-directed mutagenesis analyses. The first target was Lys^{83} (corresponding to Lys^{85} of bovine adrenal cytochrome b_{561}), that is a highly conserved residue and is locating on the cytosolic loop connecting between helices 2 and 3 and might be spatially very close to the cytosolic heme *b* prosthetic group (Supporting Information Figure S8) (*10*) and to the "motif 1" sequence (*37*). Our site-specific chemical modification studies using diethyl pyrocarbonate (DEPC) on bovine adrenal cytochrome b_{561} (*12*, *13*) and on WT-Zmb_{561} (*48*, *49*) showed that this residue had a high reactivity toward the reagent. Further, since such chemical modification caused a distinct inhibition on the fast electron acceptance from AsA, it might have a strong interaction with a negatively charged AsA molecule and is likely to have a very important mechanistic role for the rapid electron acceptance from cytosolic AsA (*12*, *13*, *47*).

The second and third targets were Ser^{118} and Trp^{122} (corresponding to Ser^{120} and Trp^{124} of the bovine adrenal cytochrome b_{561}), respectively, locating on an intravesicular loop connecting helices 3 and 4 (Supporting Information Figure S8). These two residues are part of the putative "MDA radical-binding sequence" (or "motif2"), and their conservation is extremely high among the animal and plant cyochromes b_{561} (Supporting Information Figure S5) (*10*). Since one of the heme axial ligands of the extravesicular heme cener is His^{120} (corresponding to His^{122} of the bovine adrenal cytochrome b_{561}), it is quite reasonable to consider that these might have very crucial roles for the electron donation to the MDA radical or other possible electron acceptors on the intravesicular side.

Visible Absorption Spectra of the Site-Specific Mutants and the pH-Dependent Behavior of the Final Reduction Level. All of the purified site-specific mutants (K83A, K83E, K83D, S118A, W122A-H_6) showed visible absorption spectra with peaks at 414 nm for the oxidized form and at 561, 529, and 427 nm for the dithionite-reduced form at pH 7.0 (spectra not shown), very similar to those of WT-Zmb_{561} (Figure 1B) and of bovine adrenal cytochrome b_{561} (*11*). These results suggested that all of the mutations did not affect the overall structure of Zmb_{561} molecule and, further, local structures of the immediate surroundings of the two heme *b* centers were almost intact.

For the K83A mutant, our assay using AsA as a reductant showed a significant decrease in the final heme reduction level in an acidic pH region. Results at pH 5.0 are shown for K83A (Figure 3A) in comparison with those for WT-Zmb_{561} (Figure 3B). The K83A mutant was scarcely reduced with AsA (10 mM) even after 30 min of incubation at room temperature (Figure 3A). The final AsA reduction level of the K83A mutant at

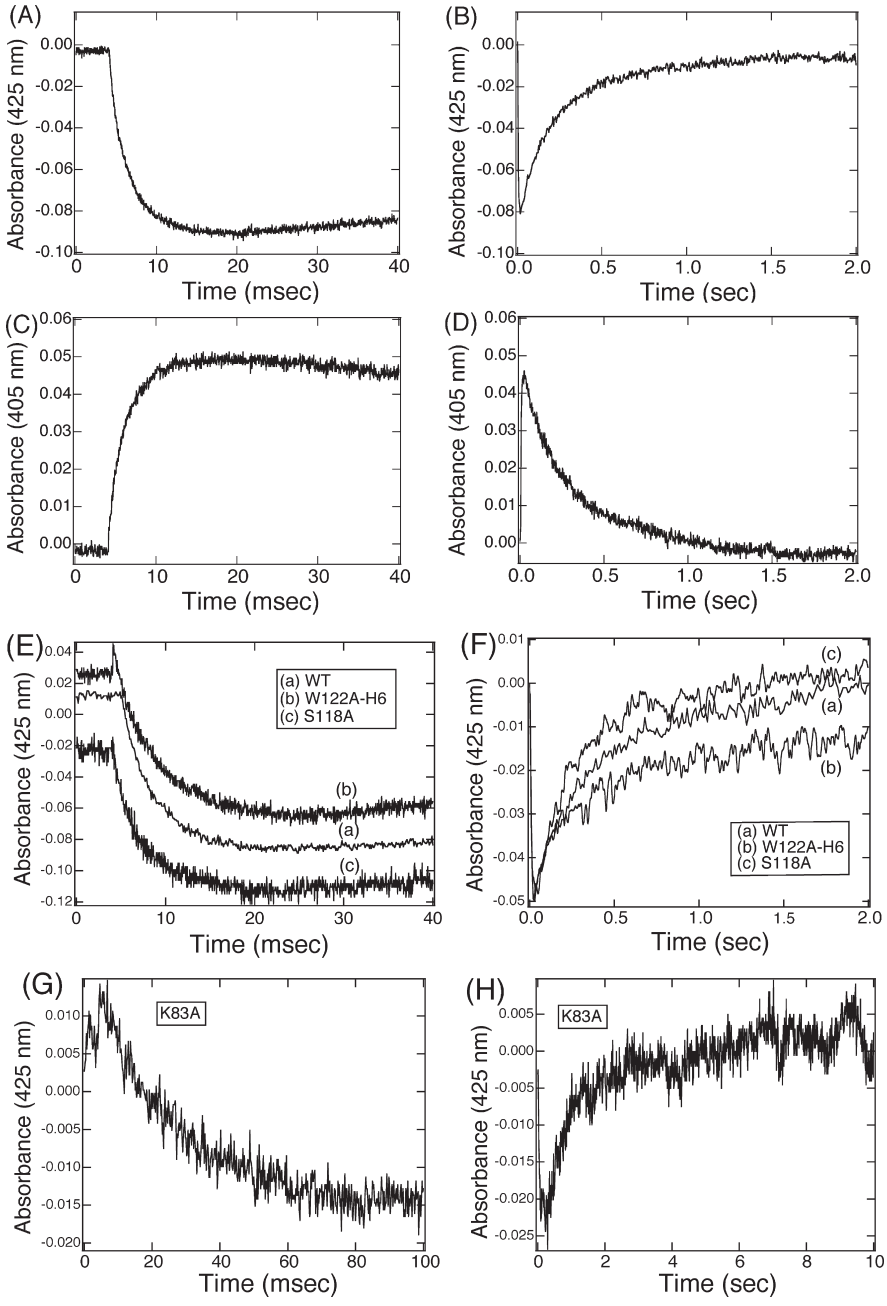

FIGURE 4: Measurements of electron transfer activities of the purified WT-Zmb_{561} to the MDA radical (A, B) and the following rereduction process (C, D) by AsA with a pulse radiolysis technique and the effects of the mutations on these electron transfer activities (E, F, G, H). Sample solutions (WT-Zmb_{561}, S118A, W122A-H_6, K83A) were each diluted with 50 mM potassium phosphate buffer (pH 7.0) containing 1.0% *n*-octyl β-glucoside and 10 mM AsA to make the final concentration to 4−6 μM. The MDA radical was generated by pulse radiation in the presence of AsA (10 mM), and the following absorbance changes at 425 nm (A) and 405 nm (B) of the purified WT-Zmb_{561} were recorded at room temperature. Recordings were continued in a longer time domain of the reaction at 425 nm (C) and 405 nm (D). In panel (E), electron-donating reactions from the reduced heme center of W122A-H_6 (b) and S118A (c) to the MDA radical were measured at 425 nm and were compared with that of WT-Zmb_{561} (a). Following rereduction processes with surrounding AsA in a longer time domain were compared similarly in panel F. In panels G and H, the electron-donating reaction from the reduced heme of K83A to the MDA radical and a following rereduction process with surrounding AsA in a longer time domain are measured similarly.

pH 5.0 was calculated as low as 25% of the dithionite-reduced level (Figure 3C). It must be noted that this lower reduction level was not due to the denaturation, since the spectrum of the dithionite-reduced form at pH 5.0 (Figure 3A) was almost identical with those of WT-Zmb_{561} measured at pH 5.0 (Figure 3B) or measured at pH 7.0 (Figure 1B). We noticed further that the K83D mutant also showed a significant lowering in the electron-accepting activity with AsA as a reductant (Figure 3C). On the other hand, the final heme reduction level of the K83E mutant was not much different from that of WT-Zmb_{561} (Figure 3C). Taken together, these results suggested that the Lys^{83} residue might have an indispensable role for the electron acceptance from AsA. However, its mechanistic roles in the electron transfer might not be so simple.

Two site-specific mutants (S118A and W122A-H_6) for the well-conserved "motif 2" sequence (*10*, *37*) showed a similar reactivity with that of WT-Zmb_{561} in the same assay, reaching to the final heme reduction level around 70% (Figure 3C). They did not show any significant pH dependency.

Table 2: Apparent Rate Constants of the Heme Oxidation by the MDA Radical and the Following Heme Rereduction by AsA in Zmb_{561} and Its Site-Specific Mutants[a]

	app oxidation rate by MDA radical ($\times 10^3$ s^{-1})			app reduction rate by AsA (s^{-1})		
cytochrome	pH 7.0	pH 6.0	pH 5.0	pH 7.0	pH 6.0	pH 5.0
WT-Zmb_{561}	0.27	0.47	0.66	2.4	5.5	4.6
S118A	0.27	0.63	0.74	3.7	5.7	4.8
W122A-H_6	0.30	0.50	1.1	3.0	2.7	5.3
K83A	0.031	ND	ND	0.60	ND	ND

[a]The apparent rate constants were means of the values obtained at two different wavelengths (425 and 405 nm; the former indicates the decrease in the reduced heme concentration, whereas the latter indicates the increase in the oxidized heme concentration). ND: not determined.

Stopped-Flow Analyses of the Site-Specific Mutants for the Electron Acceptance Activity from AsA. The electron-accepting reaction from AsA of the three Lys^{83} mutants was further analyzed by stopped-flow spectrometry to clarify the anomalous pH dependency. The absorbance changes at 427 nm after the mixing of the oxidized form of WT-Zmb_{561} (and the three K83 mutants) (final, 1 μM) with AsA (final, 8 mM) at pH 7.0 were presented against time in a logarithmic scale (Figure 5A). The results showed that the heme reduction process of K83A was much slower than that of WT-Zmb_{561}, showing a clear initial time lag even at pH 7.0. Such an initial time lag was found previously for bovine adrenal cytochrome b_{561} (*47*) and in the present study for WT-Zmb_{561} (Supporting Information Figure S12) and was pH-dependent in either case, evident only in a lower pH region (pH 5.0 or 5.5). It might be noted that the apparent initial time lag was further prolonged for K83E and K83D mutants at pH 7.0 (Figure 5A). In an acidic pH, however, both the K83E and K83D mutants showed faster electron transfer than the K83A (Figure 5B,C). For the K83A mutant, at pH 5.0, the initial time lag was further enhanced, and the resulting final reduction level decreased (Figures 4C and 5C). These stopped-flow data confirmed that the Lys^{83} residue has a very important role for the electron acceptance from AsA on the extravesicular side but its mechanism is somewhat complicated.

Pulse Radiolysis Analyses on the Mutants for the Electron Donation to the MDA Radical and Rereduction by AsA. To clarify the physiological roles of "mofif 2" (the putative "MDA-binding sequence") (*10*, *37*), we measured the electron-donating ability to the MDA radical from the reduced heme center for S118A, W122A-H_6, and K83A by a pulse radiolysis technique. Results showed that the former two "mofif 2" mutants and WT-Zmb_{561} had very similar apparent rate constants (k_{app}) to each other for the electron donation to the MDA radical (Figure 4E) at three different pH (7.0, 6.0, and 5.0) (Table 2). There was a clear tendency for these three Zmb_{561} species that the rate constant increased as pH was becoming acidic (Table 2).

In a following longer time domain in the pulse radiolysis experiments, we observed the rereduction process of the oxidized heme center (Figure 4F), caused by an intramolecular electron transfer from the cytosolic heme center to the intravesicular heme and simultaneous rereduction of the cytosolic heme by surrounding AsA in the medium. Although both processes were spectroscopically indistinguishable from each other, the apparent rate constants of the whole rereduction process were almost identical between WT-Zmb_{561} and the two mutants (S118A, W122A-H_6) (Table 2).

For a comparative purpose, we performed pulse radiolysis experiments for the K83A mutant but only at pH 7.0 (Figure 4G,H). Unexpectedly, the apparent rate constant for the electron-donating reaction to the MDA radical from the reduced heme center was found to be 3.1×10 s^{-1}, about one-ninth of the corresponding value of WT-Zmb_{561} (Table 2). On the other hand, the apparent rate constant for the rereduction of the oxidized heme center after the electron donation to the MDA radical (0.60 s^{-1}) was about one-fourth of the corresponding value of WT-Zmb_{561} (Table 2).

EPR Spectroscopy of the K83A Mutant. To evaluate the quality of our mutant sample, we measured EPR spectra of the K83A mutant as a representative example. EPR spectra of the K83A mutant measured at 5 and 15 K (with $g_z = 3.69$ and $g_z = 3.22$) (Supporting Information Figure S11B) were very similar to those of WT-Zmb_{561} (Supporting Information Figure S11A), indicating that the side-chain group of Lys^{83} did not have a direct interaction with the cytosolic heme center and, therefore, substitution of Lys^{83} to Ala residue did not affect the conformation and the electronic structures of the heme moieties.

Redox Potential Measurements of the Site-Specific Mutants. We, then, analyzed the effects of site-specific mutations at the Lys^{83} residue on the redox behavior of the heme group. The K83A mutant showed a slight lowering of the apparent midpoint potential to +45 mV (Supporting Information Figure S13A, Table 1), slightly lower than that of WT-Zmb_{561} (Figure 2B, Table 1). On the other hand, estimated values for its midpoint potentials of the higher and the lower redox components were +93 and −4 mV, respectively (Table 1). The K83E mutant also showed a similar lowering in the redox potentials; the apparent midpoint point potential was found as +37 mV and the higher and the lower redox components were estimated as +90 and −21 mV, respectively (Supporting Information Figure S13B, Table 1). The K83D mutant showed a drastic change in its redox behavior. The apparent midpoint potential lowered to as low as −36 mV, and the higher and the lower redox components were estimated as +50 and −127 mV, respectively (Supporting Information Figure S13C, Table 1). Particularly, the lower redox component was found about 140 mV lower than the corresponding value of WT-Zmb_{561}.

For a comparative purpose, we also analyzed effects of the S118A mutation. Supporting Information Figure S13D shows a slight lowering of the apparent midpoint potential to +43 mV, and the estimated midpoint potentials of the higher and the lower redox components were +102 and −13 mV, respectively (Table 1). Similarly, corresponding values of the W122A-H_6 mutant showed not much difference from those of WT-Zmb_{561} (Table 1). These results indicated that the mutations in the putative MDA radical-binding sequence did not affect significantly on the redox properties of the heme *b* centers.

DISCUSSION

Heterologous Expression of Z. mays Cytochrome b_{561}. In the present study, we succeeded in the purification of

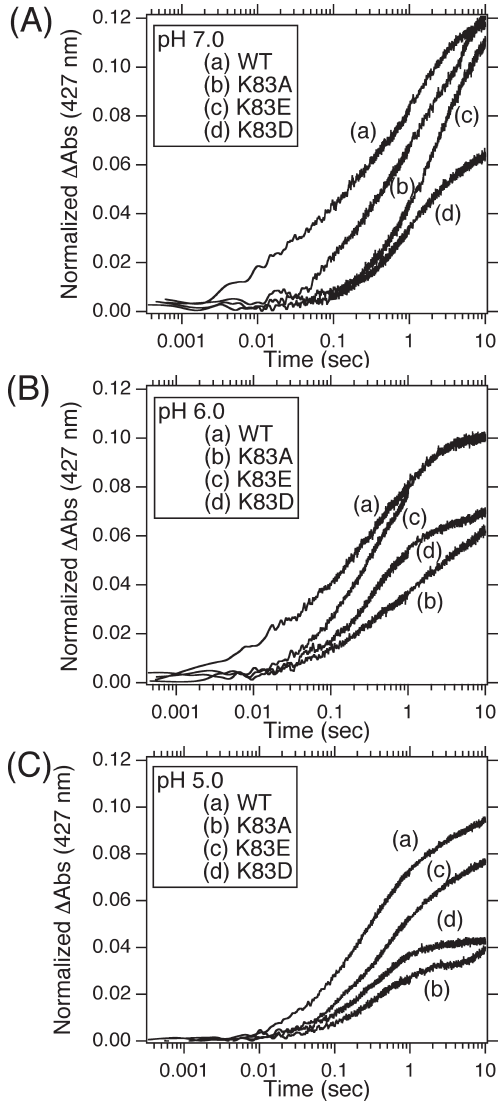

FIGURE 5: Stopped-flow analysis on the electron transfer from AsA for the purified WT-Zmb_{561} and its K83 mutants (K83A, K83D, and K83E) measured at pH 7.0 (A), pH 6.0 (B), and pH 5.0 (C). The electron acceptance reaction from AsA (final 8 mM) was measured by stopped-flow spectrometry using two solution mixing systems with a 1:1 volume ratio. The absorbance change at 427 nm was traced after mixing the oxidized WT-Zmb_{561} (a) or its mutants (K83A (b), K83E (c), K83D (d); final, 1 μM) with AsA (final, 8 mM). The normalized absorbance changes were plotted against time in a logarithmic scale. Other conditions are described in the text.

heterologously expressed maize cytochrome b_{561} (Zmb_{561}) in an intact state as judged by its visible absorption spectra (Figure 1B) and other biochemical (Figure 1A) and biophysical (Figures 2, 3) properties showing a clear resemblance to those of bovine adrenal cytochrome b_{561}. Existence of two independent heme *b* centers was inferred based on the amino acid sequence analysis (Supporting Information Figure S5) and was confirmed by EPR spectroscopy (Supporting Information Figure S11A). In the oxidized state of purified Zmb_{561}, two EPR species with different g_z values (3.69, 3.21) were clearly observed. The g_z = 3.69 species was assigned as the cytosolic heme center, whereas the g_z = 3.21 species was assigned as the intravesicular heme center, respectively, as previously assigned for bovine adrenal cytochrome b_{561} based on the DEPC modification and pulse radiolysis experiments (*4*, *11*, *14*) and the 4-PDS modification experiment (*35*). Although the *g*-value for the g_z = 3.21 species showed a slightly higher value than that of bovine adrenal cytochrome b_{561}, their spectral character and the temperature dependency were very like each other, suggesting a very similar molecular architecture around the two heme centers despite only ~32% identity in their amino acid sequences. The two EPR species with different g_z values were also observed for recombinant mouse chromaffin granule cytochrome b_{561} (g_z = 3.71, 3.27) (*41*) and for recombinant human duodenal cytochrome b_{561} (g_z = 3.7, 3.18) (*50*). Our present assignment on the heme centers is not consistent with a recent proposal by Kamensky et al. (*42*), in which the low-potential heme (the g_z = 3.69 species) was assigned to the intravesicular side on the basis of EPR spectra of the heme axial ligand mutants of recombinant bovine adrenal cytochrome b_{561}. However, our model was supported by many experimental results on bovine adrenal cytochrome b_{561} as indicated above and is in full accordance with the notion of the direction of the physiological electron transfer (i.e., cytosolic AsA, low-potential heme, high-potential heme, and intravesicular MDA radical), and therefore, we believe it is much more feasible.

The presence of a *b*-type cytochrome in *Z. mays* root was previously reported by Bérczi et al. (*27*). In their partially purified samples, a polypeptide band at about 26 kDa, very close to the theoretical molecular mass (25424.52 Da) of the cloned Zmb_{561} in the present study, was observed and seemed to be correlated with the high cytochrome b_{561} content of the fraction (*27*). However, further purification of this particular cytochrome b_{561} form was unsuccessful, and therefore, it is not clear whether this AsA-reducible *b*-type cytochrome corresponded to our present Zmb_{561} form or not.

Physiological Electron Donor and Acceptor of Z. mays Cytochrome b_{561}. The heme centers of purified Zmb_{561} could be reduced with AsA very rapidly at a neutral pH as revealed by stopped-flow studies (Supporting Information Figure S12). Further, pulse radiolysis experiments demonstrated that the reduced heme center of Zmb_{561} donated electron equivalents to MDA radical very rapidly (Figure 4A,B). The estimated midpoint potentials of the two heme centers (Figure 2, Table 1) were suitable for the redox reactions with AsA and MDA radicals. These results suggested that AsA is working as an active physiological electron donor for this cytochrome in maize cells and the AsA-regenerating system on the intravesicular side of Zmb_{561} might be actively working by utilizing the electron equivalents from cytosolic AsA, as found for bovine adrenal cytochorme b_{561} (*4*). The regenerated AsA may be coupled with other redox reaction(s) on the intravesicular side in corn plant cells. Recently, an isoform of cytochrome b_{561} from *A. thaliana* was found to be expressed on vacuole membranes based on a cell fractionation study (*29*−*31*). AsA has been known to be present in plant tissues quite a lot, especially in root tissues, and is thought to act as a substrate for many enzymes, such as AsA-dependent dioxygenases for the synthesis of hydroxyproline-containing proteins, flavonoids and important hormones (*51*), ascorbate peroxidase for scavenging reactive oxygen species (*52*), and ascorbate oxidase for a putative role in oxygen management (*53*). However, the histochemical silver staining study showed that AsA was not present in significant amounts in vacuoles (*54*). Since the subcellular and tissue-specific localization of Zmb_{561} has not yet been clarified, we need further investigations on the distribution and physiological role(s) of this particular plant cytochrome b_{561}.

Strong pH Dependency of the Electron Acceptance from AsA. Stopped-flow analyses of both Zmb_{561} (present study) and

bovine adrenal cytochrome b_{561} (*47*) upon electron acceptance from AsA showed a significant time lag in an acidic pH region (Supporting Information Figure S12). Such a retardation of the electron acceptance from AsA in a lower pH region was previously ascribed to the electrochemistry of AsA (*47*), in which a proton has to be removed from the C2-hydroxyl group of AsA before the occurrence of (or concurrently with) the electron donation to the electron acceptor (*55*, *56*). We postulated that (one of) the heme axial His residues on the cytosolic side has such a role to accept a proton from a bound AsA molecule ("the concerted proton/electron transfer mechanism") (*57*); such a specific role for the proton acceptance from AsA could explain the specific inactivation of the electron acceptance from AsA by a site-specific DEPC modification of the axial His residue most reasonably (*47*, *57*).

Interestingly, feasibility of the deprotonated histidyl ligand(s) in the oxidation of AsA by cytochrome b_{561} by a proton-coupled electron transfer mechanism (*58*) has been examined experimentally using (TPP)Fe^{3+}−imidazolate complexes and an ascorbate derivative (*59*). They found that deprotonation of the imidazole ligand caused a faster (more than a factor of 10) electron transfer reaction and concluded that the electron transfer occurred most likely by hydrogen atom transfer (HAT) (*59*). HAT is a type of proton-coupled electron transfer reaction in which a proton and an electron were transferred in a single kinetic step from one donor to one acceptor (*58*).

Thus, the present results showed that the concerted proton/electron transfer mechanism might be operative in Zmb_{561} as well and could be a common mechanism in the members of the diheme-containing cytochrome b_{561} protein family. If one considered the lower conservation of the amino acid sequences between *Z. mays* and bovine adrenal cytochromes b_{561}, it might be reasonable to conclude that the mechanism is maintained by only a limited number of conserved residues on the cytosolic side, which include two heme axial His residues (His^{86} and His^{159}), Lys^{83}, Arg^{72}, and Tyr^{71}.

Roles of the Highly Conserved Lys^{83} Residue on the Cytosolic Side. Previous site-specific chemical modification studies on bovine adrenal cytochrome b_{561} using DEPC suggested the importance of the Lys^{85} residue for the quick electron acceptance from AsA (*12*, *13*). Indeed, the Lys^{85} residue is well conserved among animal and plant cytochromes b_{561} (*10*). Our recent study on WT-Zmb_{561} by employing the same strategy indicated that Lys^{83} (corresponding to Lys^{85} of bovine adrenal cytochrome b_{561}) had similar high reactivity toward DEPC and resulting N-carbethoxylation of the Lys^{83} residue was responsible partly for the inhibition of the electron acceptance from AsA (*48*, *49*). To clarify the mechanistic role(s) of this positively charged residue during the electron-accepting process, we constructed three mutants, K83A, K83D, and K83E. Stopped-flow analyses for these purified mutants showed that the duration of the time lag was much longer than that of WT-Zmb_{561} at pH 7.0, resulting in a significant retardation of the electron transfer (Figure 5A). Substitution of the Lys^{83} residue, which has a positive charge at pH 7.0, to the Ala residue would cause a loss of +1 charge, which would remove the electrostatic interaction between the side-chain group and a negatively charged AsA molecule, leading to a retardation of electron transfer from AsA. Substitution to the Glu or Asp residue will cause a total charge change of −2, which would cause an electrostatic repulsion between the side-chain group and an AsA molecule, leading to a further retardation (Figure 5A) and lowering of the final reduction level (Figure 3C).

The electrostatic interaction alone, however, cannot explain the present results. It might be noted that the final heme reduction levels of three K83 mutants with AsA as a reductant were pH-dependent and significantly different from each other (Figures 3C and 5A−C). Both K83D and K83A mutants showed a significant decrease in the final heme reduction level at pH 5.0, whereas the wild-type protein and the K83E mutant did not (Figure 3C). These observations seemed to indicate that, at pH 5.0, where the electrostatic effects might become weakened, other factors would become dominated. One may focus on the K83D mutant, which has a much lower reduction potential for the low potential heme than the other cytochromes. This most likely explains its poor extent of reduction by AsA, especially at low pH where AsA will have a higher reduction potential. The fact that the extent of reduction is less than 50% might suggest that AsA is unable to reduce the low potential heme at all. The same logic may be applicable for the K83A mutant at pH 5.0, where it has the lowest extent of reduction with AsA (Figure 3C), suggesting that it may have a very low redox potential at this pH, although we did not make measurement at pH 5.0.

However, the redox potential of a heme group within the protein moiety (or the electron transfer reaction in the protein moiety) would be controlled by many factors including charges, hydrophobicity, and other structural factors. We should be careful about the size effect of the side-chain group. Substitutions of the Lys^{83} residue to a smaller side-chain group (Ala or Asp) may trigger a series of conformational changes leading to the significant alterations in the redox properties (see later discussion). Taken together, the present results were consistent with the notion that, at a neutral pH, the positive charge at the Lys^{83} residue has a very important role for the interaction with a negatively charged AsA molecule and such electrostatic interactions would be a primary factor in the initial phase of the electron transfer from AsA, as previously proposed (*47*).

Initial Time Lag and Roles of the Putative AsA-Binding Sequence. The exact nature and the cause of the initial time lag in the electron acceptance from AsA observed in an acidic pH region are not well understood, as discussed in previous sections. The most likely explanation would be as follows: the deprotonation of the heme axial His residue is a slow process, and this accounts for the time lag appearing in the initial phase. Such deprotonation process may be initiated by the binding of AsA to the substrate-binding site. As one possible alternative scenario, the time lag might indicate the duration required for the binding of AsA to the substrate-binding site and for the bound AsA molecule to be reoriented in a proper direction for the efficient electron transfer. In any case, Lys^{83} might be participating in the binding process of AsA to the substrate-binding site. On the other hand, our recent study indicated that substitution of one conserved basic residue (Arg^{72}) locating in the same cytosolic loop to Ala residue abolished the characteristic pH-dependent initial time lag almost completely, resulting in the fast electron transfer even at an acidic pH (Rahman et al., unpublished observation). This unexpected observation, which was in disagreement with the observation by Su and Han (*60*), suggested that, upon the electron acceptance from AsA to the cytosolic heme center, multiple and complex interactions among a negatively charged AsA molecule and other surrounding amino acid residues are operative. Similar studies focusing on other conserved residues are currently underway.

Physiological Roles of Motif 2 on the Intravesicular Side. "Motif 2" (the SLHSW sequence) residing in the

hydrophilic loop between helix 3 and helix 4 is the best and almost completely conserved sequence among the members of the cytochrome b_{561} family in animal and plant species (*10*, *37*). Compared to the "motif 1" sequence on the cytosolic side, its conservation is rather high. Therefore, this sequence was predicted to have some important functions on the intravesicular side of cytochrome b_{561}, most likely for the electron donation to the MDA radical (*10*). In the present study, we constructed two mutants (S118A, W122A-H_6) to investigate the structural and mechanistic role(s) of the sequence.

To confirm whether such mutations on the intravesicular side would not affect the structure and function of the cytosolic heme center, the visible absorption spectra of the oxidized and dithionite-reduced forms of these mutants were compared with those of WT-Zmb_{561}. We found that the visible absorption spectra of both mutants showed not much difference from those of WT-Zmb_{561}. Further, the final heme reduction level of both mutants with AsA as a reductant showed values higher than 60% irrespective to the pH condition. Similarly, redox potential measurements showed that neither of the two mutations affected the midpoint potentials of their two heme centers significantly (Table 1). Therefore, we concluded that these two mutants could be used as good models to investigate the role of the "motif 2" sequence in the electron-donating activity to the MDA radical on the intravesicular side.

Unexpectedly, neither of the two mutations affected the electron transfer reaction to the MDA radical at all in the pulse radiolysis experiment (Table 2). One may propose that the absence of significant effects on the two mutants indicates that this highly conserved "motif 2" sequence does not have a direct link to the electron-donating reaction from the reduced heme center to the MDA radical but only has a structural role for the stability around the intravesicular heme center. In the case of the S118A mutant, the size of the two side-chain groups did not change so much, and therefore, it might be reasonable to observe not much influence. However, in the case of the W122A mutant, there should be a significant alteration in the size of side-chain groups upon the substitution. We still do not have a reasonable answer for these results at this moment. As one possibility, a single mutation in the "motif 2" sequence might not be sufficient to cause a significant change in the rigid intravesicular heme center. In another possibility, strictness of the sequence except for His^{120} might not be so important at least for the redox properties of the intravesicular heme center. In the latter scenario, the "motif 2" sequence might have an unknown physiologically important role(s). It should be noted that CYBASC1 (an isoform of *A. thaliana* cytochrome b_{561}) was reported to have a transmembrane ferrireductase activity (*39*). Further, other members of the cytochrome b_{561} family in animals and plants were also reported to have some ferrireductase activities more or less (*16*, *39*, *60*, *61*). Taken together, members of the cytochromes b_{561} family in general may have an electron-donating activity against various electron acceptors (such as ferricyanide, ferric−EDTA, and ferric−citrate) but with very low substrate specificity. However, in the strict sense, there had been no direct proof that cytochrome b_{561} donated electron equivalents directly to the ferric electron acceptors mentioned above. Since all previous measurements were conducted using cultured cells, the possibility that other endogenous small redox molecule(s) might be working as a mediator could not be completely ruled out. In this case, the "motif 2" sequence might be important for such molecular recognitions.

Unusual Behavior of the K83A Mutant in Pulse Radiolysis Analyses. Finally, we should discuss the unusual behavior of the K83A mutant in the pulse radiolysis experiment. The slowed apparent rate constant for the rereduction process of the oxidized heme with AsA (Figure 4H, Table 2) was consistent with the results from the stopped-flow analyses (Figure 5A) and, therefore, might be very reasonable. However, the slowed apparent rate constant for the initial electron donation to the MDA radical from the reduced heme of the K83A mutant (Figure 4G, Table 2) was very difficult to explain. EPR spectra of the K83A mutant indicated that the intravesicular heme center was very similar to that of WT-Zmb_{561} (Supporting Information Figure S11), suggesting that the mutation of Lys^{83} on the cytosolic side did not cause any tertiary structural change around the heme centers and, therefore, there should be no structural defect to perform the electron donation to the MDA radical. As one plausible explanation, we are considering "a concerted electron transfer mechanism", where a concurrent replenishment with an electron equivalent from the cytosolic heme center might be required to conduct the efficient electron donation from the intravesicular heme center to the MDA radical. However, one may claim that our previous observation on the DEPC-treated bovine adrenal cytochrome b_{561}, where the electron donation to MDA radical was not much different from that of the untreated cytochrome b_{561} (*12*), is not consistent with this view. Probably, the DEPC treatment would not cause any appreciable defect for the intramolecular electron transfer due to the hydrophilic nature of the carbethoxy group or its sufficient size. On the other hand, for the K83A mutant, such intramolecular electron transfer might be damaged severely due to a substitution to a smaller hydrophobic side-chain group. Such a structural damage might also be responsible partly for the extended initial time lag and the lower reduction level observed in the stopped-flow experiments of the K83 mutants, as discussed in the previous section. To clarify the nature of the intramolecular electron transfer and to evaluate our present proposal, further detailed studies for other K83 mutants are being planed. Such studies would clarify whether we need some revisions on our current view for the transmembrane electron transfer mechanism of cytochrome b_{561} or not.

Conclusions. In conclusion, we found that recombinant Zmb_{561} obtained by a heterologous expression system using yeast *P. pastoris* cells could utilize the AsA/MDA radical as the physiological electron donor/acceptor. We found further that a concerted proton/electron transfer mechanism might be operative in Zmb_{561} as well upon the electron acceptance from AsA to the cytosolic heme center and that Lys^{83} has a very important role for the binding of AsA and the electron transfer via electrostatic interactions. It was postulated that Lys^{83} might also be responsible for the intramolecular electron transfer to the intravesicular heme center based on the unusual behavior for the K83A mutant in the pulse radiolysis experiments. On the other hand, we could not obtain any clear evidence to indicate that two conserved residues, Ser^{118} and Trp^{122}, in the intravesicular loop have major roles for the interactions with the MDA radical.

SUPPORTING INFORMATION AVAILABLE

Molecular cloning of *Z. mays* cytochrome b_{561} cDNA, preparation of the *Z. mays* b_{561}/pPICZB construct and expression of recombinant *Z. mays* cytochrome b_{561} in yeast *P. pastoris* cells, and supporting figures. This material is available free of charge via the Internet at http://pubs.acs.org.

REFERENCES

1. Njus, D., Knoth, J., Cook, C., and Kelley, P. M. (1983) Electron transfer across the chromaffin granule membrane. *J. Biol. Chem. 258*, 27–30.
2. Kelley, P. M., and Njus, D. (1986) Cytochrome b_{561} spectral changes associated with electron transfer in chromaffin-vesicle ghosts. *J. Biol. Chem. 261*, 6429–6432.
3. Kent, U. M., and Fleming, P. J. (1987) Purified cytochrome b_{561} catalyzes transmembrane electron transfer for dopamine β-hydroxylase and peptidyl glycine α-amidating monooxygenase activities in reconstituted systems. *J. Biol. Chem. 262*, 8174–8178.
4. Kobayashi, K., Tsubaki, M., and Tagawa, S. (1998) Distinct roles of two heme centers for transmembrane electron transfer in cytochrome b_{561} from bovine adrenal chromaffin vesicles as revealed by pulse radiolysis. *J. Biol. Chem. 273*, 16038–16042.
5. Eipper, B. A., Mains, R. E., and Glembotski, C. C. (1983) Identification in pituitary tissue of a peptide α-amidation activity that acts on glycine-extended peptides and requires molecular oxygen, copper, and ascorbic acid. *Proc. Natl. Acad. Sci. U.S.A. 80*, 5144–5148.
6. Russell, J. T. (1987) The secretory vesicle in processing and secretion of neuropeptides, in Current Topics in Membranes and Transport, pp 277−312, Academic Press, New York.
7. Prigge, S. T., Kolhekar, A. S., Eipper, B. A., Mains, R. E., and Amzel, L. M. (1997) Amidation of bioactive peptides: The structure of peptidylglycine α-hydroxylating monooxygenase. *Science 278*, 1300–1305.
8. Iliadi, K. G., Avivi, A., Iliadi, N. N., Knight, D., Korol, A., Nevo, E., Taylor, P., Moran, M. F., Kamyshev, N. G., and Boulianne, G. L. (2008) nemy encodes a cytochrome b_{561} that is required for *Drosophila* learning and memory. *Proc. Natl. Acad. Sci. U.S.A. 105*, 19986–19991.
9. Perin, M. S., Fried, V. A., Slaughter, C. A., and Südhof, T. C. (1988) The structure of cytochrome b_{561}, a secretory vesicle-specific electron transport protein. *EMBO J. 7*, 2697–2703.
10. Okuyama, E., Yamamoto, R., Ichikawa, Y., and Tsubaki, M. (1998) Structural basis for the electron transfer across the chromaffin vesicle membranes catalyzed by cytochrome b_{561}: Analyses of cDNA nucleotide sequences and visible absorption spectra. *Biochim. Biophys. Acta 1383*, 269–278.
11. Tsubaki, M., Nakayama, M., Okuyama, E., Ichikawa, Y., and Hori, H. (1997) Existence of two heme B centers in cytochrome b_{561} from bovine adrenal chromaffin vesicles as revealed by a new purification procedure and EPR spectroscopy. *J. Biol. Chem. 272*, 23206–23210.
12. Tsubaki, M., Kobayashi, K., Ichise, T., Takeuchi, F., and Tagawa, S. (2000) Diethylpyrocarbonate-modification abolishes fast electron accepting ability of cytochrome b_{561} from ascorbate but does not influence on electron donation to monodehydroascorbate radical: Distinct roles of two heme centers for electron transfer across the chromaffin vesicle membranes. *Biochemistry 39*, 3276–3284.
13. Takeuchi, F., Kobayashi, K., Tagawa, S., and Tsubaki, M. (2001) Ascorbate inhibits the carbethoxylation of two histidyl and one tyrosyl residues indispensable for the transmembrane electron transfer reaction of cytochrome b_{561}. *Biochemistry 40*, 4067–4076.
14. Takeuchi, F., Hori, H., Obayashi, E., Shiro, Y., and Tsubaki, M. (2004) Properties of two distinct heme centers of cytochrome b_{561} from bovine chromaffin vesicles studied by EPR, resonance Raman, and ascorbate reduction assay. *J. Biochem. 135*, 53–64.
15. Asada, A., Kusakawa, T., Orii, H., Agata, K., Watanabe, K., and Tsubaki, M. (2002) Planarian cytochrome b_{561}: Conservation of a six-transmembrane structure and localization along the central and peripheral nervous system. *J. Biochem. 131*, 175–182.
16. Mckie, A. T., Barrow, D., Latunde-Dada, G. O., Rolfs, A., Sager, G., Mudaly, E., Mudaly, M., Richardson, C., Barlow, D., Bomford, A., Peters, T. J., Raja, K. B., Shirali, S., Hediger, M. A., Farzaneh, F., and Simpson, R. J. (2001) An iron-regulated ferric reductase associated with the absorption of dietary iron. *Science 291*, 1755–1759.
17. McKie, A. T. (2008) The role of Dcytb in iron metabolism: An update. *Biochem. Soc. Trans. 36*, 1239–1241.
18. Ponting, C. P. (2001) Domain homologues of dopamine β-hydroxylase and ferric reductase: roles for iron metabolism in neurodegenerative disorders? *Hum. Mol. Genet. 10*, 1853–1858.
19. Asard, H., Terol-Alcayde, J., Preger, V., Del Favero, J., Verelst, W., Sparla, F., Pérez-Alonso, M., and Trost, P. (2000) *Arabidopsis thaliana* sequence analysis confirms the presence of cyt *b*-561 in plants: Evidence for a novel protein family. *Plant Physiol. Biochem. 38*, 905–912.
20. Verelst, W., Kapila, J., de Almeida Engler, J., Stone, J. M., Caubergs, R. J., and Asard, H. (2004) Tissue-specific expression and developmental regulation of cytochrome *b*561 genes in *Arabidopsis thaliana* and *Raphanus sativus*. *Physiol. Plant. 120*, 312–318.
21. Preger, V., Pesaresi, A., Pupillo, P., and Trost, P. (2001) Ascorbate-independent electron transfer between cytochrome b_{561} and a 27 kDa ascorbate peroxidase of bean hypocotyls. *Protoplasma 217*, 137–145.
22. Nanasato, Y., Akashi, K., and Yokota, A. (2005) Co-expression of cytochrome *b*561 and ascorbate oxidase in leaves of wild watermelon under drought and high light conditions. *Plant Cell Physiol. 46*, 1515–1524.
23. Asard, H., Kapila, J., Verelst, W., and Bérczi, A. (2001) Higher-plant plasma membrane cytochrome *b*561: A protein in search of a function. *Protoplasma 217*, 77–93.
24. Asard, H., Venken, M., Caubergs, R., Reijnders, W., Oltmann, F. L., and De Greef, J. A. (1989) *b*-Type cytochromes in higher plant plasma membranes. *Plant Physiol. 90*, 1077–1083.
25. Scagliarini, S., Rotino, L., Bäurle, I., Asard, H., Pupillo, P., and Trost, P. (1998) Initial purification study of the cytochrome b_{561} of bean hypocotyl plasm membrane. *Protoplasma 205*, 66–73.
26. Trost, P., Bèrczi, A., Sparla, F., Sponza, G., Marzadori, B., Asard, H., and Pupillo, P. (2000) Purification of cytochrome *b*561 from bean hypocotyls plasma membrane. Evidence for the presence of two heme centers. *Biochim. Biophys. Acta 1468*, 1–5.
27. Bérczi, A., Lüthje, S., and Asard, H. (2001) *b*-type cytochromes in plasma membranes of *Phaseolus vulgaris* hypocotyls, *Arabidopsis thaliana* leaves, and *Zea mays* roots. *Protoplasma 217*, 50–55.
28. Bérczi, A., Caubergs, R. J., and Asard, H. (2003) Partial purification and characterization of an ascorbate-reducible *b*-type cytochrome from the plasma membrane of *Arabidopsis thaliana* leaves. *Protoplasma 221*, 47–56.
29. Shimaoka, T., Ohnishi, M., Sazuka, T., Mitsuhashi, N., Hara-Nishimura, I., Shimazaki, K.-i., Maeshima, M., Yokota, A., Tomizawa, K.-I., and Mimura, T. (2004) Isolation of intact vacuoles and proteomic analysis of tonoplast from suspension-cultured cells of *Arabidopsis thaliana*. *Plant Cell Physiol. 45*, 672–683.
30. Griesen, D., Su, D., Bérczi, A., and Asard, H. (2004) Localization of an ascorbate-reducible cytochrome *b*561 in the plant tonoplast. *Plant Physiol. 134*, 726–734.
31. Preger, V., Scagliarini, S., Pupillo, P., and Trost, P. (2005) Identification of an ascorbate-dependent cytochrome *b* of the tonoplast membrane sharing biochemical features with members of the cytochrome *b*561 family. *Planta 220*, 365–375.
32. Daly, R., and Hearn, M. T. W. (2005) Expression of heterologous proteins in *Pichia pastoris*: A useful experimental tool in protein engineering and production. *J. Mol. Recognit. 18*, 119–138.
33. Markwell, M. A. K., Haas, S. M., Tolbert, N. E., and Bieber, L. L. (1981) Protein determination in membrane and lipoprotein sampled: Manual and automated procedures. *Methods Enzymol. 72*, 296–303.
34. Laemmli, U. K. (1970) Cleavage of structural proteins during the assembly of the head of bacteriophage T_4. *Nature 227*, 680–685.
35. Takeuchi, F., Hori, H., and Tsubaki, M. (2005) Selective perturbation of the intravesicular heme center of cytochrome *b*561 by cysteinyl modification with 4,4′-dithiodipyridine. *J. Biochem. 138*, 751–762.
36. Dutton, P. L. (1978) Redox potentiometry: Determination of midpoint potentials of oxidation-reduction components of biological electron-transfer systems. *Methods Enzymol. 54*, 411–435.
37. Tsubaki, M., Takeuchi, F., and Nakanishi, N. (2005) Cytochrome *b*561 protein family: Expanding roles and versatile transmembrane electron transfer abilities as predicted by a new classification system and protein sequence motif analyses. *Biochim. Biophys. Acta 1753*, 174–190.
38. Kyte, J., and Doolittle, R. F. (1982) A simple method for displaying the hydropathic character of a protein. *J. Mol. Biol. 157*, 105–132.
39. Bérczi, A., Su, D., and Asard, H. (2007) An *Arabidopsis* cytochrome *b*561 with *trans*-membrane ferrireductase capability. *FEBS Lett. 581*, 1505–1508.
40. Su, D., May, J. M., Koury, M. J., and Asard, H. (2006) Human erythrocyte membranes contain a cytochrome b_{561} that may be involved in extracellular ascorbate recycling. *J. Biol. Chem. 281*, 39852–39859.
41. Bérczi, A., Su, D., Lakshminarasimhan, M., Vargas, A., and Asard, H. (2005) Heterologous expression and site-directd mutagenesis of an ascorbate-reducible cytochrome *b*561. *Arch. Biochem. Biophys. 443*, 82–92.
42. Kamensky, Y., Liu, W., Tsai, A.-L., Kulmacz, R. J., and Palmer, G. (2007) The axial ligation and stoichiometry of heme centers in adrenal cytochrome b_{561}. *Biochemistry 46*, 8647–8658.
43. Zacharius, R. M., Zell, T. E., Morrison, J. H., and Woodlock, J. J. (1969) Glycoprotein staining following electrophoresis on acrylamide gels. *Anal. Biochem. 30*, 148–152.

44. Apps, D. K., Boisclair, M. D., Gavine, F. S., and Pettigrew, G. W. (1984) Unusual redox behaviour of cytochrome *b*-561 from bovine chromaffin granule membranes. *Biochim. Biophys. Acta 764*, 8–16.
45. Flatmark, T., and Terland, O. (1971) Cytochrome b_{561} of the bovine adrenal chromaffin granules. A high potential *b*-type cytochrome. *Biochim. Biophys. Acta 253*, 487–491.
46. Kamensky, Y. A., Arutjunjan, A. M., Konstantinov, A. A., Moroz, I. A., and Burbaev, D. S. (1989) Multiple forms of cytochrome *b* in adrenal chromaffin granule, in International Symposium "Molecular Organization of Biological Structures", pp A2−A7, Moscow, Russia.
47. Takigami, T., Takeuchi, F., Nakagawa, M., Hase, T., and Tsubaki, M. (2003) Stopped-flow analyses on the reaction of ascorbate with cytochrome *b*561 purified from bovine chromaffin vesicle membanes. *Biochemistry 42*, 8110–8118.
48. Nakanishi, N., Rahman, M. M., Sakamoto, Y., Miura, M., Takeuchi, F., Park, S.-Y., and Tsubaki, M. (2009) Inhibition of electron acceptance from ascorbate by the specific *N*-carbethoxylations of maize cytochrome b_{561}: A common mechanism for the transmembrane electron transfer in cytochrome b_{561} protein family, *J. Biochem.* (in press).
49. Rahman, M. M., Nakanishi, N., Fujito, M., Miura, M., Hase, T., Park, S.-Y., Hori, H., and Tsubaki, M. (2008) Inhibition of the electron transfer of plant cytochrome *b*561 by the modification with diethylpyrocarbonate: In search of a common mechanism for the transmembrane electron transfer from ascorbate, in MHS2008. International Synmposium on Micro-NanoMechatoronics and Human Science, pp 157−162, IEEE, Nagoya.
50. Oakhill, J. S., Marritt, S. J., Gareta, E. G., Cammack, R., and McKie, A. T. (2008) Functional characterization of human duodenal cytochrome *b* (Cybrd1): Redox properties in relation to iron and ascorbate metabolism. *Biochim. Biophys. Acta 1777*, 260–268.
51. Arrigoni, O., and De Tullio, M. C. (2002) Ascorbic acid: Much more than just an antioxidant. *Biochim. Biophys. Acta 1569*, 1–9.
52. Shigeoka, S., Ishikawa, T., Tamoi, M., Miyagawa, Y., Takeda, T., Yabuta, Y., and Yoshimura, K. (2002) Regulation and function of ascorbate peroxidase isoenzymes. *J. Exp. Bot. 53*, 1305–1319.
53. De Tullio, M. C., Ciraci, S., Liso, R., and Arrigoni, O. (2007) Ascorbic acid oxidase is dynamically regulated by light and oxygen. A tool for oxygen management in plants? *J. Plant Physiol. 164*, 39–46.
54. Liso, R., De Tullio, M. C., Ciraci, S., Balestrini, R., La Rocca, N., Bruno, L., Chiappetta, A., Bitonti, M. B., Bonfante, P., and Arrigoni, O. (2004) Localization of ascorbic acid, ascorbic acid oxidase, and glutathione in roots of *Cucurbita maxima* L. *J. Exp. Bot. 55*, 2589–2597.
55. Njus, D., and Kelley, P. M. (1993) The secretory-vesicle ascorbate-regenerating system: A chain of concerted H^+/e^--transfer reactions. *Biochim. Biophys. Acta 1144*, 235–248.
56. Njus, D., Wigle, M., Kelley, P. M., Kipp, B. H., and Schlegel, H. B. (2001) Mechanism of ascorbic acid oxidation by cytochrome b_{561}. *Biochemistry 40*, 11905–11911.
57. Nakanishi, N., Takeuchi, F., and Tsubaki, M. (2007) Histidine cycle mechanism for the concerted proton/electron transfer from ascorbate to the cytosolic heme *b* center of cytochrome b_{561}: A unique machinery for the biological transmembrane electron transfer. *J. Biochem. 142*, 553–560.
58. Mayer, J. M. (2004) Proton-coupled electron transfer: A reaction chemist's view. *Annu. Rev. Phys. Chem. 55*, 363–390.
59. Waaren, J. J., and Mayer, J. M. (2008) Hydrogen atom transfer reactions of iron-porphyrin-imidazole complexes as models for histidine-ligated heme reactivity. *J. Am. Chem. Soc. 130*, 2774–2776.
60. Su, D., and Asard, H. (2006) Three mammalian cytochrome *b*561 are ascorbate-dependent ferrireductases. *FEBS J. 273*, 3722–3734.
61. Vargas, J. D., Herpers, B., Mckie, A. T., Gledhill, S., McDonnell, J., van der Heuvel, M., Davies, K. E., and Ponting, C. P. (2003) Stromal cell-derived receptor 2 and cytochrome *b*561 are functional ferric reductase. *Biochim. Biophys. Acta 1651*, 116–123.